Published in final edited form as:
Magn Reson Med. 2013 May ; 69(5): 1443–1450. doi:10.1002/mrm.24355.

EPR oxygen imaging and hyperpolarized ^{13}C MRI of pyruvate metabolism as non-invasive biomarkers of tumor treatment response to a glycolysis inhibitor 3-bromopyruvate

Shingo Matsumoto[1], **Keita Saito**[1], **Hironobu Yasui**[1,2], **H. Douglas Morris**[3], **Jeeva P. Munasinghe**[3], **Martin Lizak**[3], **Hellmut Merkle**[3], **Jan Henrik Ardenkjaer-Larsen**[4,5], **Rajani Choudhuri**[1], **Nallathamby Devasahayam**[1], **Sankaran Subramanian**[1], **Alan P. Koretsky**[3], **James B. Mitchell**[1], and **Murali C. Krishna**[1]

[1]Radiation Biology Branch, Center for Cancer Research, National Cancer Institute, NIH, Bethesda, MD, USA

[2]Laboratory of Radiation Biology, Department of Environmental Veterinary Sciences, Graduate School of Veterinary Medicine, Hokkaido University, Sapporo, Japan

[3]National Institute of Neurological Disorder and Stroke, NIH, Bethesda, MD, USA

[4]GE Healthcare, Broendby, Denmark

[5]Technical University of Denmark, Lyngby, Denmark

Abstract

The hypoxic nature of tumors results in treatment resistance and poor prognosis. To spare limited oxygen for more crucial pathways, hypoxic cancerous cells suppress mitochondrial oxidative phosphorylation, and promote glycolysis for energy production. Thereby, inhibition of glycolysis has the potential to overcome treatment resistance of hypoxic tumors. Here, EPR imaging was used to evaluate oxygen dependent efficacy on hypoxia-sensitive drug. The small molecule 3-bromopyruvate (3-BP) blocks glycolysis pathway by inhibiting hypoxia inducible enzymes, and enhanced cytotoxicity of 3-BP under hypoxic conditions has been reported *in vitro*. However, the efficacy of 3-BP was substantially attenuated in hypoxic tumor regions (pO_2 < 10 mmHg) *in vivo* using squamous cell carcinoma (SCCVII)-bearing mouse model. Metabolic MRI studies using hyperpolarized ^{13}C-labeled pyruvate showed that monocarboxylate transporter-1 (MCT1) is the major transporter for pyruvate and the analog 3-BP in SCCVII tumor. The discrepant results between *in vitro* and *in vivo* data were attributed to biphasic oxygen dependent expression of MCT1 *in vivo*. Expression of MCT1 was enhanced in moderately hypoxic (8–15 mmHg) tumor regions, but down regulated in severely hypoxic (< 5 mmHg) tumor regions. These results emphasize the importance of non-invasive imaging biomarkers to confirm the action of hypoxia-activated drugs.

Keywords

3-bromopyruvate; EPR imaging; HIF-1; hyperpolarized ^{13}C MRI; MCT1; tumor hypoxia

Correspondence should be addressed to: Murali C. Krishna, Radiation Biology Branch, Center for Cancer Research, National Cancer Institute, NIH Building 10, Room B3B69, NIH, Bethesda, MD 20892-1002, USA Tel: +1-301-496-7511, Fax: +1-301-480-2238, murali@helix.nih.gov.

We all authors have no conflicts of interest to be disclosed .

Introduction

Cancer treatment has not been uniformly successful when directed against a single site or a pathway. This is especially the case in situations where the malignant cells have numerous genetic and biochemical abnormalities (1). These abnormalities confer phenotypes associated with drug resistance such as drug inactivation, drug export, enhanced DNA damage repair, increased expression of anti-apoptotic and prosurvival pathways, energy consuming activities that utilize significant ATP (adenosine triphosphate) (2–3). Tumor cells exhibit the Warburg phenomenon of aerobic glycolysis for energy generation and obtain as much as 50% of their ATP by metabolizing glucose directly to lactate even in the presence of oxygen, unlike normal tissue that produces most of their ATP by metabolizing the glucose to carbon dioxide and water in mitochondria by an oxygen-dependent pathway (4–5). Although the underlying molecular mechanisms of the shift in energy production from oxidative phosphorylation to glycolysis are extremely complex and not well defined, the resultant up-regulation of glucose uptake and its metabolic pathway confer great opportunity for diagnoses and treatments of cancer by targeting the aerobic glycolysis (4). Inhibitors of glycolysis may restore drug resistance by decreasing ATP levels needed for active processes involved in drug resistance and increase intracellular drug levels (6–11). Furthermore, many solid tumors outgrow the blood supply and therefore have regions with chronic and cycling hypoxia (12–14). Cancer cells harbored within these hypoxic regions try to survive the hypoxic microenvironment by preserving limited amount of oxygen for more critical physiological pathways (4,15) and generate energy by aerobic glycolysis. The glycolysis inhibitor 3-bromo pyruvate (3-BP) has been used successfully in cells and in a variety of tumor xenografts, and found to be efficacious in overcoming drug resistance (10–11,16–20). The pyruvate analog 3-BP is a small molecule inhibitor of hexokinase II, an enzyme which is highly expressed in malignant cells compared with normal cells (21) and catalyzes the initial metabolic step in the conversion of glucose to glucose-6-phosphate during the glycolysis, resulting in a rapid depletion of ATP, making it a promising anti-tumor drug (22–23). Pedersen and colleagues have shown that 3-BP is effective in killing liver tumors implanted in rats and rabbits (22–23). A synergistic anti-cancer effect of 3-BP was observed when it was given with geldanamycin, a heat-shock protein 90 inhibitor, in the transgenic pancreatic tumor model mice (16–17). Interestingly, the synergistic effect of 3-BP and geldanamycin was highly enhanced when cancer cells were incubated under hypoxic conditions. In *in vitro* experiments, Xu et al. have found that 3-BP was preferentially cytotoxic to cancer cells under hypoxia than normoxia (10).

The preferential hypoxic cytotoxicity of 3-BP implies a potential to overcome treatment resistance of hypoxic tumor cells against radiotherapy and other chemotherapeutic drugs. In order to further examine the oxygen dependent anti-tumor effect of 3-BP *in vivo*, we utilized electron paramagnetic resonance imaging (EPRI) to map the tumor pO_2 to determine the oxygen dependence in the response to 3-BP (13) in a squamous cell carcinoma (SCCVII) tumor model bearing in mice, and unexpectedly found that the cytotoxic effect of 3-BP was significantly lower in hypoxic tumor regions with pO_2 <10 mmHg than in more oxygenated areas. The underlying mechanisms were examined by histological analysis and hyperpolarized MRI of ^{13}C-labeled pyruvate study (of note, 3-BP is a mimic of pyruvate) showing the limited expression of monocarboxylate transporter 1 (MCT1), a major transporter up-taking both 3-BP and pyruvate into cells, in severely hypoxic tumor regions. These results suggest the importance of evaluating and predicting effectiveness of molecular targeted drugs *in vivo* using non-invasive imaging biomarkers to select optimal treatment for the individual tumor and to minimize resistance.

Methods

Chemicals

Hexokinase II inhibitor 3-bromopyruvate (3-BP) and MCT1 inhibitor a-cyano-4-hydroxycinnamate (CHC) were purchased from Sigma (St. Louis, MO). [1-^{13}C]-pyruvic acid was purchased from Cambridge Isotope Laboratories Inc. (Andover, MA) and Isotec Inc. (Miamisburg, OH). Triarylmethyl EPR probe (TAM) was obtained from GE Healthcare (London, GB).

Cell culture

SCCVII mouse squamous cell carcinoma cells (obtained from Dr. T. Phillips, UCSF, San Francisco, CA and was tested in 2011 by RADIL using a panel of microsatellite markers) were routinely cultured in RPMI medium with 10% fetal calf serum.

Animal experiments

All animal experiments were carried out in compliance with the *Guide for the care and use of laboratory animal resources* (National Research Council, 1996) and the experimental protocols were approved by the National Cancer Institute Animal Care and Use Committee. Female C3H/Hen mice were supplied by the Frederick Cancer Research Center, Animal Production (Frederick, MD). Murine SCCVII solid tumors were formed by injecting 5×10^5 cells subcutaneously into right hind legs of mice. The experiments were initiated when tumors grew to approximately 1 cm in size. In the imaging experiments, mice were anaesthetized by isoflurane inhalation (4 % for induction and 1-2 % for maintaining anesthesia) and positioned prone with their tumor-bearing legs placed inside the resonator. During EPRI and MRI measurements, the breathing rate of mouse was monitored with a pressure transducer (SA, Instruments Inc.) and maintained at 60 ± 15 breaths per minutes. Core body temperature was maintained at 34–37 °C with a flow of warm air for EPR imaging and with a warm water pad for MRI study.

Combined EPR oxygen imaging and anatomic MRI

Technical details of the EPRI scanner operating at 300 MHz, radio-frequency (RF) coil design, data acquisition based on the single point imaging (SPI) modality, image reconstruction, and the oximetry calculation procedure were described in the earlier reports(13,24–27). Briefly, the SPI sequence is a pure phase-encoding spectral and spatial imaging technique. The free induction decays (FIDs) following the excitation pulse (60 ns for the smaller parallel coil resonator (24) and 80 ns for the larger coil, 80 W) were sampled using a fast analog digital converter (200 M samples/s). The smaller (17 mm inner diameter) RF coil was used for imaging of tumor bearing mouse leg, and the larger one (25 mm i.d.) was used for imaging of lower body of mouse including both tumor leg and contralateral normal leg. Repetition time (TR) of 8.0 3s with 70° flip angle satisfies the Ernst angle condition for steady state magnetization. The FIDs were collected under a nested looping of the x, y, z gradients and each time point in the FID underwent phase modulation enabling 3D spatial encoding. Since FIDs last for a few microseconds, we can generate a sequence of T_2^* mapping, which allowed pixel-wise estimation of tissue pO_2 (13,26). The spatial resolution was 1.6-1.8 mm defined by the gradient strength (max gradient = 1.4 G/cm), the number of k-samples (elements in k-space = 19 × 19 × 19 or 23 × 23 × 23), and time delay (600–1100 ns) after the excitation pulse (27). The pixel resolution was digitally enhanced in order to coregister with MRI images.

Anatomic MRI measurements were performed with a 7 T scanner controlled with ParaVision 5.0 (Bruker Bio-Spin MRI GmbH). After a quick assessment of the sample position by a fast low-angle shot (FLASH) tripilot sequence, T_2-weighted anatomical

images were obtained using a fast spin echo sequence (RARE) with an echo time (TE) of 13 ms, TR of 2,500 ms, 14 or 16 slices with 2 mm thickness, RARE factor 8, in plane resolution of 0.109 or 0.125 mm, and acquisition time of 80 s. Details of corregistration method to combine EPRI and MRI images have been reported previously (13).

^{13}C MRI of hyperpolarized ^{13}C-laveled pyruvate metabolism

Samples of [1-^{13}C] pyruvic acid (30 μL) containing 15 mM of OX063 and 2.5 mM of the gadolium chelate ProHance (Bracco Diagnostics, Milano, Italy) were polarized at 3.35 T and 1.4 K in the Hypersense DNP polarizer (Oxford Instruments), according to the manufacturer's instructions. After 1-1.5 hr, the hyperpolarized sample was rapidly dissolved in 4.5 mL of a superheated alkaline buffer comprising 40 mM 4-(2-hydroxyethyl)-1-piperazineethanesulfonic acid (HEPES), 30 mM of NaCl and 100 mg/L ethylendiaminetetraacetic acid (EDTA). NaOH was added to the dissolution buffer to be pH 7.4 after mixture with [1-^{13}C] pyruvic acid. Hyperpolarized [1-^{13}C] pyruvate solution (12 μL/g body weight) was intravenously injected through a catheter placed in the tail vein of mouse.

Hyperpolarized ^{13}C MRI studies were performed on a 4.7T scanner (Bruker Bio-Spin MRI GmbH) using a 17-mm home-built ^{13}C solenoid coil placed inside of a saddle coil for ^{1}H. The ^{13}C two-dimensional spectroscopic images were acquired 30 s after the start of pyruvate injection from a 28 x 28 mm field of view in a 8 mm coronal slice through the tumor, with matrix size of 16 x 16, spectral width of 6010 Hz, TR 75 ms, 250 μs Gaussian excitation pulse with a flip angle of 5°. The total time required to acquire an image was 19.2 s.

Ex vivo clonogenic colony assay

Immediately after EPRI and following anatomic MRI scans, 5 or 10 mg/kg body weight of 3-BP was administrated into the mice. Twenty four hours later, mice were euthanized by breathing carbon dioxide gas and 3–4 mm cube tumor biopsy samples were obtained from the specific locations of the tumor based on the 3D pO_2 maps with anatomic guidance by MRI. The tumor tissues were immediately minced by scissors and digested by 0.2% collagenase/0.02% deoxyribonuclease solution to be single-cell suspensions. Cells were counted and seeded in culture dishes to be concentrations of 200–10,000 cells/dish for colony formation. Ten to fourteen days after, colonies were stained by a crystal violet and numbers of colonies were counted. Percentage of cell survival was normalized by the number of colonies of tumor tissues obtained from non-treated control mice to be 100% survival.

Immunohistochemistry

Tumor bearing mice were euthanized and perfused with 10 ml of 4 % paraformaldehyde. Tumor tissues were excised and fixed with 4 % paraformaldehyde over night, frozen with Tissue-Tek® O.C.T. compound (Sakura Finetek U.S.A. Inc., Torrance, CA) on cold ethanol, and 10 μm thick sections were obtained. After blocking non-specific binding sites with serum-free protein block (Dako North America Inc., Carpinteria, CA), the slides were covered by HIF-1a antibody (Novus Biologicals, Littleton, CO; 1:1000) or MCT1 antibody (Santa Cruz Biotech., Santa Cruz, CA; 1:250) overnight at 4 °C. The sections were incubated with Alexa Fluor 546 anti-rabbit antibody (Invitrogen, Carlsbad, CA; 1:500), and were mounted on Prolong Gold antifade reagent with DAPI (Invitrogen). Fluorescence microscopic observation was performed using an Axiovert 200 inverted fluorescent microscope (Carl Zeiss).

Results

Glycolysis inhibitor 3-BP suppresses SCCVII tumor growth

Activation of glycolysis has been widely reported in SCC tumors in preclinical models and patients (13,28). To investigate the effect of 3-BP on growth of the SCCVII tumor bearing mouse, 10 mg/kg of 3-BP was daily administrated 10 days after tumor implantation when tumor size was 1.0–1.2 cm. As shown in Figure 1, 3-BP significantly delayed the SCC tumor growth compared with PBS treated control tumor group of mice. These observations are in agreement with earlier reports using this agent to treat tumors in various *in vitro* and *in vivo* preclinical models (10,16–17,22).

Three-dimensional oxygen maps in a SCCVII tumor from EPRI and anatomic images from MRI

To investigate the dependence of tumor oxygen in responding to the cytotoxic effects of 3-BP, we examined the spatial distribution of oxygen in the tumor bearing mouse, using EPR imaging with the paramagnetic tracer TAM, which through collisional interaction with tissue oxygen can report on tissue oxygen status quantitatively and non-invasively (13). While EPRI provides oxygen distribution, it intrinsically lacks anatomic details. To overcome this problem, we developed a sequential EPRI and MRI imaging system using a resonator assembly tuned to the common frequency of 300 MHz for both modalities (13). Figure 2 shows seven adjacent slices of coronal and axial T_2-weighted anatomic images from MRI, and corresponding pO_2 images from EPRI after administration of the oxygen-sensitive paramagnetic tracer TAM in the SCCVII tumor-bearing mice. Each MRI slice was 2 mm thick and the corresponding pO_2 image slice was selected from the 3D image data of EPR oxygen imaging. Heterogeneous pO_2 distribution ranging from 0-40 mmHg was observed throughout the tumor (marked green line in Fig. 2) exhibiting a significant hypoxic regions with pO_2 <10 mmHg as shown by blue color in pO_2 maps. The pO_2 maps of tumor generated by EPRI therefore have the ability to guide the sampling of cells from different regions of the tumor from the tumor bearing animal treated with 3-BP, based on the a priori knowledge of their oxygen levels.

3-BP favors killing relatively oxygenated tumor cells more than severely hypoxic cells in vivo

To investigate oxygen dependent cytotoxicity of 3-BP *in vivo*, two different doses of 3-BP were administrated into mice after sequential EPRI and MRI scans. Twenty four hours later, 3–4 biopsy samples were obtained from each tumor. The locations of biopsy samples (3–4 mm cube) were guided by pO_2 maps from EPRI with anatomic guidance from MRI to have: 1) severely hypoxic regions with pO_2 <5 mmHg; 2) moderate hypoxic regions with pO_2 ranging 5–15 mmHg; and 3) well oxygenated tumor regions with pO_2 >15 mmHg. The biopsy samples were digested to obtain a single cell suspension. These cells were plated for macroscopic colony forming ability and tumor cell survival was analyzed using a clonogenic colony assay. A schematic of methodology is provided in Figure 3A. In contrast with reports from *in vitro* studies by other groups where a “hypoxic toxin” like cytotoxicity profile was attributed to 3-BP (10,16), results from the present pO_2 image guided cell survival studies show that, 3-BP exhibits stronger cytotoxic effects (<10% cell survival) in relatively well oxygenated tumor regions (pO_2 >10 mmHg) compared to severely hypoxic tumor regions, where 3-BP suppressed tumor cell survival to an extent of 60% which was less than that seen in well oxygenated regions (Fig. 3B). We did not observe significant dose dependency on the cytotoxic effective of 3-BP with the tested doses (5–10 mg/kg).

3-BP is up taken into SCCVII cells via MCT1

The glycolysis inhibitor 3-BP is a halogenated analog of pyruvate, and might be up taken into tumor cells via MCT families, especially MCT1 (29). To test the dependence of 3-BP on the MCT transporters to exert cytotoxicity, we carried out *in vitro* studies in SCCVII cells exposed to 3-BP in the presence and absence of CHC, a potent inhibitor of MCT1. Results from this study show that the concentration dependent cytotoxicity of 3-BP was retarded significantly in the presence of the MCT1 inhibitor CHC in the cell culture medium (Fig. 4A), suggesting that 3-BP is taken up into SCCVII cells via the MCT1 transporter. To further investigate the possible contribution of MCT1 to the tumor uptake of pyruvate analogs *in vivo*, metabolic MRI of hyperpolarized ^{13}C-labeled pyruvate was applied to the SCCVII tumor model with or without inhibition of MCT1 transporter with CHC. The recent development of MRI methods to probe tumor biochemical and metabolic profile using ^{13}C labeled pyruvate as the tracer and monitor its intracellular conversion to various metabolites offers a unique opportunity to examine the transport of pyruvate in tumor cells in tumor bearing mice. Figure 4B shows a typical ^{13}C MR spectroscopic profile in the SCCVII tumor after injection of hyperpolarized ^{13}C labeled pyruvate. Strong ^{13}C-lactate signal buildup was observed a few seconds following ^{13}C-pyruvate signal arrival in tumor region, suggesting that intravenously injected pyruvate was taken up into the cells, and immediately metabolized into mainly lactate in tumors. Therefore, if MCT1 is the major transporter of pyruvate analogs in the SCCVII tumors, its inhibition with CHC should suppress the conversion of pyruvate to lactate. Representative 2D spectroscopic images of ^{13}C-pyruvate and its metabolites obtained 30 seconds after pyruvate injection with or without pre-administration of CHC are shown in Figure 4C. Inhibition of MCT1 with CHC pre-treatment resulted in a significant suppression of pyruvate-to-lactate conversion (Fig. 4D). Of note, the dose of CHC used in this experiment is that of cancer treatment and may not completely suppress the pyruvate transport via MCT1 in mice. These results suggest that MCT1 is a major transporter of pyruvate and may serve as a surrogate biomarker for the transport of 3-BP in tumor cells.

MCT1 overexpressed in tumor regions with moderate hypoxia, but decreased in severely hypoxic regions in vivo

While overexpression of MCT1 has been reported in malignant tissues, conflicting observations were reported on the oxygen dependency of MCT1 expression between *in vitro* and *in vivo* studies (see the discussion section for details) (30–33). To investigate the oxygen dependency of MCT1 expression *in vivo*, we conducted immuno-staining of MCT1 and HIF-1a expression in the tumor tissue slice corresponding to the particular slice of three dimensional pO_2 map obtained from EPRI based on the anatomic guide from MRI. From the pO_2 image guided histologic experiments, a biphasic oxygen dependency of MCT1 and HIF-1a expression was observed (Fig. 5). In the tumor regions with moderate hypoxia (pO_2 = 5–15 mmHg, marked by green line) surrounding severely hypoxic core (yellow line), increased expression of MCT1 was observed as well as overexpression of HIF-1a in the moderately hypoxic regions. However, the expression level of MCT1 was clearly down regulated in the severely hypoxic tumor regions, especially where pO_2 was found to be below 2–3 mmHg. On the other hand, HIF-1 expression was high even in severely hypoxic tumor regions when the severely hypoxic area is relatively small (mouse 1). Suppressed expression of HIF-1 was observed only if the size of severely hypoxic regions were beyond 2–3 mm (mouse 2) that is similar to the biphasic expression pattern of HIF-1 near necrotic tumor regions reported in both pre-clinical models and human tumors (34–36). It should be noted that a decrease in the MCT1 expression in the severely hypoxic regions was substantial and much steeper compared to that of HIF-1a, and the diminished MCT1 expression was observed in the tumor regions with $pO_2 < 8$–12 mmHg. Collectively, the limited efficacy of the glycolysis inhibitor 3-BP in severely hypoxic tumor regions *in vivo*

revealed by EPRI may be attributed to the reduced expression of MCT1, as well as the possible poor delivery of chemotherapeutics in these hypoxic tumor regions.

Discussion

Inhibition of glycolysis, which was found to be elevated in a wide range of cancer cell types, is promising in cancer therapy. Molecular targets of the glycolysis inhibitor 3-BP were suggested to be hexokinase II and GAPDH, which are both hypoxia-inducible enzymes (9,23). This may partially explain the higher cytotoxicity of 3-BP under hypoxia as reported previously in cell culture studies (10). However, using non-invasive and quantitative EPR imaging of tumor oxygen status, we found that the efficacy of 3-BP was diminished in severely hypoxic areas of tumor, which can be explained by the down regulation of MCT1, a major transporter of 3-BP in the severely hypoxic tumor regions. In addition, MTT assays or flow cytometry assessment of apoptosis was used in the previously reported *in vitro* studies, while clonogenic colony assay in this study. The MTT assay measures cell growth; hence any agent that slows growth could be incorrectly considered “cytotoxic.” Agents or conditions can be cytostatic, but not necessarily cytotoxic. If hypoxic conditions slowed the growth of cells compared to cells maintained under normoxia the assay would report cytotoxicity for the hypoxic conditions. Assessment of apoptosis as a sole indicator of cytotoxicity is problematic in that cells can die through other processes including mitotic-linked death. The clonogenic assay takes into account all types of cell death and is therefore a better assay to determine the cytotoxicity of an agent or experimental conditions.

Monocarboxylate transpoters (MCTs) are involved in both aerobic and anaerobic metabolism. Within the identified 14 isoforms in mammals, MCT4 is transcriptionally regulated by HIF-1a and has been considered to be the major hypoxia-responsible isoform (37). On the other hand, MCT1 is ubiquitously expressed in various tissues, and has been considered to be responsible for aerobic metabolism (37). However, recent reports present conflicting data on the oxygen dependency of MCT1 expression (30–31,33,36). Hypoxic-incubation has been reported to stimulate MCT1 expression in rat cortical astrocytes, human adipocytes, and heart of zebrafish (30–33). In solid tumors, MCT1 was identified to be responsible for symbiotic energy fuel exchange between oxidative and hypoxic/glycolytic tumor cells. Sonveaux et al. demonstrated that oxidative tumor cells expressed higher levels of MCT1 than MCT4 and that the hypoxic (positive for HIF-1a and pimonidazole) subpopulation poorly expresses MCT1 (32). Thus, lactate extruded by hypoxic/glycolytic tumor cells through MCT4 was proposed to be taken up by oxygenated tumor cells by MCT1 to fuel oxidative metabolism. However Koukourakis et al. have reported a co-localized higher expression of surrogate hypoxia markers HIF-1a/lactate dehydrogenase (LDH) and MCT1 in colorectal adenocarcinomas from patients (38). Biphasic oxygen-dependency of MCT1 expression as shown in this study may partially explain the differing levels of reports on MCT1 expression in the various studies (30–33).

Two possible reasons for the biphasic oxygen dependency of MCT1 expression or the discrepant observations on MCT1 expression pattern may exist. The first reason is the biphasic time dependency of MCT1 overexpression under hypoxia. Several groups have reported that relatively short-termed (< 48 hrs) exposure to hypoxia stimulates MCT1 expression but the overexpression of MCT1 diminishes in the case of long-term (96 hrs ~ 3 weeks) hypoxic incubation (30–31,33). Solid tumors are now well known to be exposed to cycles of short-termed hypoxia/re-oxygenation, named as transient or cycling tumor hypoxia (12,14,39–40). Therefore, it is likely that MCT1 expression may be enhanced in tumor regions with cycling hypoxia, but be down regulated in chronically hypoxic tumor cores.

Second, the oxygen dependency of hypoxia markers such as HIF-1a and pimonidazole, which have been widely used to identify the hypoxic areas, is not straightforward *in vivo*. These markers were found to be absent in severely hypoxic tumor regions (35–36). HIF-1 is a master protein regulating cell response to oxygen concentration changes in both physiological and pathological situations. When pO_2 falls below 15 mmHg, cells try to adapt to the hypoxic microenvironment by activating HIF-1. However in tumors, Janssen et al. reported no significant correlation between the staining of exogenous hypoxic marker pimonidazole and HIF-1a expression in human head-and heck tumors (34). Colocalization of pimonidazole and HIF-1a was only 0-25%. Pimonidazole staining, where binding steeply increased at pO_2 <10 mmHg, rapidly increased at 80 μm apart from the nearest tumor blood vessel and its peak distributed around 150-200 μm from vessels, while HIF-1a distribution was more homogeneous and its peak was closer to blood vessels around 40–100 μm (or no clear peak). Sobhanifar and colleagues in an extensive study observed this discrepant phenomenon in various xenograft tumors and biopsy samples from cervical cancer patients, and concluded that nutrient deprivation seems to be largely responsible for the reduced HIF-1a expression in the most hypoxic regions, especially perinecrotic regions (36). In addition to the nutrient gradient, acidic microenvironment in tumors likely contributes the reduced HIF-1 level in hypoxic but viable areas. Tumor pH decreases to the range of 6.2–7.4 dependent on the distance from blood vessels, and expressions of HIF-1 regulating enzymes including glucose tranporter-1 (GLUT-1), carbonic anhydrase 9 (CA9), and LDH-A are all strongly suppressed at below pH 6.5 (41). MCT1 expression might not be transcriptionally controlled by HIF-1a, but more likely be regulated indirectly via its downstream enzyme LDH-A and resultant accumulated lactate, which is known to promote MCT1 expression (31,42). In a previous study using the same SCCVII tumor model, lactate accumulated to a higher extent in the moderately hypoxic regions but not in the tumor regions with severely hypoxia (13). In contrast with other hypoxic markers such as HIF-1a and pimonidazole, EPR based oximetry does not suffer from viability of cells, local pH or enzymatic activity in the tumor, making EPRI desirable tool for evaluating effect of tumor oxygen status on cancer treatment response.

Results in Figure 5 combined with previous reports suggest that maximum MCT1 expression may peak in “moderately” hypoxic tumor regions. Chronically hypoxic cells in tumor are usually distant from functional blood vessels and are consequently exposed to lower concentrations of the chemotherapeutic agents than cells in close to capillaries (43–44). Combination of such concentration gradient of 3-BP and biphasic oxygen dependency of MCT1 expression may result in the complicated oxygen dependency of treatment effect of 3-BP as shown in Figure 3B. In this hyperpolarized ^{13}C MRI studies, we measured difference in pyruvate metabolism in independent groups of mice with or without MCT1 inhibition. Multiple injections of hyperpolarized pyruvate and following ^{13}C MRI before and after MCT1 inhibitor in the same animal would make it feasible to show the distribution of MCT1 transporter within tumor. The pyruvate-to-lactate flux is affected by various factors including blood perfusion, LDH activity, coenzyme NAD^+/NADH concentrations, the size of endogenous lactate pool, and cell viability. Seth et al also reported that activation of mitochondrial oxidative phosphorylation by dichloroacetate reduced the pyruvate-to-lactate flux in a lung tumor xenograft (45). Such capability of the hyperpolarized ^{13}C MRI combined with various transporter inhibitors expands its applications to provide surrogate biomarkers for predicting and evaluating treatment response.

Acknowledgments

This research was supported by the Intramural Research Program, Center for Cancer Research, National Cancer Institute, NIH. We appreciate staffs in Mouse Imaging Facility (MIF) of NIH for help to conduct this study.

References

1. Vogelstein B, Kinzler KW. Cancer genes and the pathways they control. Nat Med. 2004; 10(8):789–799. [PubMed: 15286780]
2. Longley DB, Johnston PG. Molecular mechanisms of drug resistance. J Pathol. 2005; 205(2):275–292. [PubMed: 15641020]
3. Wilson TR, Longley DB, Johnston PG. Chemoresistance in solid tumours. Ann Oncol. 2006; 17 (Suppl 10):x315–324. [PubMed: 17018746]
4. Gatenby RA, Gillies RJ. Why do cancers have high aerobic glycolysis? Nat Rev Cancer. 2004; 4(11):891–899. [PubMed: 15516961]
5. Warburg O. On the origin of cancer cells. Science. 1956; 123(3191):309–314. [PubMed: 13298683]
6. Bhardwaj V, Rizvi N, Lai MB, Lai JC, Bhushan A. Glycolytic enzyme inhibitors affect pancreatic cancer survival by modulating its signaling and energetics. Anticancer Res. 2010; 30(3):743–749. [PubMed: 20392992]
7. Ihrlund LS, Hernlund E, Khan O, Shoshan MC. 3-Bromopyruvate as inhibitor of tumour cell energy metabolism and chemopotentiator of platinum drugs. Mol Oncol. 2008; 2(1):94–101. [PubMed: 19383331]
8. Pedersen PL. The cancer cell's "power plants" as promising therapeutic targets: an overview. J Bioenerg Biomembr. 2007; 39(1):1–12. [PubMed: 17404823]
9. Pereira da Silva AP, El-Bacha T, Kyaw N, dos Santos RS, da-Silva WS, Almeida FC, Da Poian AT, Galina A. Inhibition of energy-producing pathways of HepG2 cells by 3-bromopyruvate. Biochem J. 2009; 417(3):717–726. [PubMed: 18945211]
10. Xu RH, Pelicano H, Zhou Y, Carew JS, Feng L, Bhalla KN, Keating MJ, Huang P. Inhibition of glycolysis in cancer cells: a novel strategy to overcome drug resistance associated with mitochondrial respiratory defect and hypoxia. Cancer Res. 2005; 65(2):613–621. [PubMed: 15695406]
11. Zhou Y, Tozzi F, Chen J, Fan F, Xia L, Wang J, Gao G, Zhang A, Xia X, Brasher H, Widger W, Ellis LM, Weihua Z. Intracellular ATP levels are a pivotal determinant of chemoresistance in colon cancer cells. Cancer Res. 2012; 72(1):304–314. [PubMed: 22084398]
12. Dewhirst MW. Relationships between cycling hypoxia, HIF-1, angiogenesis and oxidative stress. Radiat Res. 2009; 172(6):653–665. [PubMed: 19929412]
13. Matsumoto S, Hyodo F, Subramanian S, Devasahayam N, Munasinghe J, Hyodo E, Gadisetti C, Cook JA, Mitchell JB, Krishna MC. Low-field paramagnetic resonance imaging of tumor oxygenation and glycolytic activity in mice. J Clin Invest. 2008; 118(5):1965–1973. [PubMed: 18431513]
14. Yasui H, Matsumoto S, Devasahayam N, Munasinghe JP, Choudhuri R, Saito K, Subramanian S, Mitchell JB, Krishna MC. Low-field magnetic resonance imaging to visualize chronic and cycling hypoxia in tumor-bearing mice. Cancer Res. 2010; 70(16):6427–6436. [PubMed: 20647318]
15. Kim JW, Tchernyshyov I, Semenza GL, Dang CV. HIF-1-mediated expression of pyruvate dehydrogenase kinase: a metabolic switch required for cellular adaptation to hypoxia. Cell Metab. 2006; 3(3):177–185. [PubMed: 16517405]
16. Cao X, Bloomston M, Zhang T, Frankel WL, Jia G, Wang B, Hall NC, Koch RM, Cheng H, Knopp MV, Sun D. Synergistic antipancreatic tumor effect by simultaneously targeting hypoxic cancer cells with HSP90 inhibitor and glycolysis inhibitor. Clin Cancer Res. 2008; 14(6):1831–1839. [PubMed: 18347186]
17. Cao X, Jia G, Zhang T, Yang M, Wang B, Wassenaar PA, Cheng H, Knopp MV, Sun D. Non-invasive MRI tumor imaging and synergistic anticancer effect of HSP90 inhibitor and glycolysis inhibitor in RIP1-Tag2 transgenic pancreatic tumor model. Cancer Chemother Pharmacol. 2008; 62(6):985–994. [PubMed: 18253734]
18. Ganapathy-Kanniappan S, Vali M, Kunjithapatham R, Buijs M, Syed LH, Rao PP, Ota S, Kwak BK, Loffroy R, Geschwind JF. 3-bromopyruvate: a new targeted antiglycolytic agent and a promise for cancer therapy. Curr Pharm Biotechnol. 2010; 11(5):510–517. [PubMed: 20420565]

19. Mathupala SP, Ko YH, Pedersen PL. Hexokinase-2 bound to mitochondria: cancer's stygian link to the "Warburg Effect" and a pivotal target for effective therapy. Semin Cancer Biol. 2009; 19(1): 17–24. [PubMed: 19101634]
20. Pedersen PL. Warburg, me and Hexokinase 2: Multiple discoveries of key molecular events underlying one of cancers' most common phenotypes, the "Warburg Effect", i.e. elevated glycolysis in the presence of oxygen. J Bioenerg Biomembr. 2007; 39(3):211–222. [PubMed: 17879147]
21. Kim W, Yoon JH, Jeong JM, Cheon GJ, Lee TS, Yang JI, Park SC, Lee HS. Apoptosis-inducing antitumor efficacy of hexokinase II inhibitor in hepatocellular carcinoma. Mol Cancer Ther. 2007; 6(9):2554–2562. [PubMed: 17876052]
22. Geschwind JF, Ko YH, Torbenson MS, Magee C, Pedersen PL. Novel therapy for liver cancer: direct intraarterial injection of a potent inhibitor of ATP production. Cancer Res. 2002; 62(14): 3909–3913. [PubMed: 12124317]
23. Ko YH, Smith BL, Wang Y, Pomper MG, Rini DA, Torbenson MS, Hullihen J, Pedersen PL. Advanced cancers: eradication in all cases using 3-bromopyruvate therapy to deplete ATP. Biochem Biophys Res Commun. 2004; 324(1):269–275. [PubMed: 15465013]
24. Devasahayam N, Subramanian S, Murugesan R, Cook JA, Afeworki M, Tschudin RG, Mitchell JB, Krishna MC. Parallel coil resonators for time-domain radiofrequency electron paramagnetic resonance imaging of biological objects. J Magn Reson. 2000; 142(1):168–176. [PubMed: 10617448]
25. Devasahayam N, Subramanian S, Murugesan R, Hyodo F, Matsumoto K, Mitchell JB, Krishna MC. Strategies for improved temporal and spectral resolution in in vivo oximetric imaging using time-domain EPR. Magn Reson Med. 2007; 57(4):776–783. [PubMed: 17390350]
26. Matsumoto K, Subramanian S, Devasahayam N, Aravalluvan T, Murugesan R, Cook JA, Mitchell JB, Krishna MC. Electron paramagnetic resonance imaging of tumor hypoxia: enhanced spatial and temporal resolution for in vivo pO2 determination. Magn Reson Med. 2006; 55(5):1157–1163. [PubMed: 16596636]
27. Subramanian S, Devasahayam N, Murugesan R, Yamada K, Cook J, Taube A, Mitchell JB, Lohman JA, Krishna MC. Single-point (constant-time) imaging in radiofrequency Fourier transform electron paramagnetic resonance. Magn Reson Med. 2002; 48(2):370–379. [PubMed: 12210946]
28. Lonneux M, Hamoir M, Reychler H, Maingon P, Duvillard C, Calais G, Bridji B, Digue L, Toubeau M, Gregoire V. Positron emission tomography with [18F]fluorodeoxyglucose improves staging and patient management in patients with head and neck squamous cell carcinoma: a multicenter prospective study. J Clin Oncol. 2010; 28(7):1190–1195. [PubMed: 20124179]
29. Harris T, Eliyahu G, Frydman L, Degani H. Kinetics of hyperpolarized 13C1-pyruvate transport and metabolism in living human breast cancer cells. Proc Natl Acad Sci U S A. 2009; 106(43): 18131–18136. [PubMed: 19826085]
30. Ngan AK, Wang YS. Tissue-specific transcriptional regulation of monocarboxylate transporters (MCTs) during short-term hypoxia in zebrafish (Danio rerio). Comp Biochem Physiol B Biochem Mol Biol. 2009; 154(4):396–405. [PubMed: 19709642]
31. Perez de Heredia F, Wood IS, Trayhurn P. Hypoxia stimulates lactate release and modulates monocarboxylate transporter (MCT1, MCT2, and MCT4) expression in human adipocytes. Pflugers Arch. 2010; 459(3):509–518. [PubMed: 19876643]
32. Sonveaux P, Vegran F, Schroeder T, Wergin MC, Verrax J, Rabbani ZN, De Saedeleer CJ, Kennedy KM, Diepart C, Jordan BF, Kelley MJ, Gallez B, Wahl ML, Feron O, Dewhirst MW. Targeting lactate-fueled respiration selectively kills hypoxic tumor cells in mice. J Clin Invest. 2008; 118(12):3930–3942. [PubMed: 19033663]
33. Vega CR, Sachleben LJ, Gozal D, Gozal E. Differential metabolic adaptation to acute and long-term hypoxia in rat primary cortical astrocytes. J Neurochem. 2006; 97(3):872–883. [PubMed: 16573648]
34. Janssen HL, Haustermans KM, Sprong D, Blommestijn G, Hofland I, Hoebers FJ, Blijweert E, Raleigh JA, Semenza GL, Varia MA, Balm AJ, van Velthuysen ML, Delaere P, Sciot R, Begg AC. HIF-1A, pimonidazole, and iododeoxyuridine to estimate hypoxia and perfusion in human head-and-neck tumors. Int J Radiat Oncol Biol Phys. 2002; 54(5):1537–1549. [PubMed: 12459383]

35. Kizaka-Kondoh S, Konse-Nagasawa H. Significance of nitroimidazole compounds and hypoxia-inducible factor-1 for imaging tumor hypoxia. Cancer Sci. 2009; 100(8):1366–1373. [PubMed: 19459851]
36. Sobhanifar S, Aquino-Parsons C, Stanbridge EJ, Olive P. Reduced expression of hypoxia-inducible factor-1alpha in perinecrotic regions of solid tumors. Cancer Res. 2005; 65(16):7259–7266. [PubMed: 16103077]
37. Chiche J, Brahimi-Horn MC, Pouyssegur J. Tumour hypoxia induces a metabolic shift causing acidosis: a common feature in cancer. J Cell Mol Med. 2010; 14(4):771–794. [PubMed: 20015196]
38. Koukourakis MI, Giatromanolaki A, Harris AL, Sivridis E. Comparison of metabolic pathways between cancer cells and stromal cells in colorectal carcinomas: a metabolic survival role for tumor-associated stroma. Cancer Res. 2006; 66(2):632–637. [PubMed: 16423989]
39. Matsumoto S, Yasui H, Mitchell JB, Krishna MC. Imaging cycling tumor hypoxia. Cancer Res. 2010; 70(24):10019–10023. [PubMed: 21159626]
40. Matsumoto S, Batra S, Saito K, Yasui H, Choudhuri R, Gadisetti C, Subramanian S, Devasahayam N, Munasinghe JP, Mitchell JB, Krishna MC. Antiangiogenic agent sunitinib transiently increases tumor oxygenation and suppresses cycling hypoxia. Cancer Res. 2011; 71(20):6350–6359. [PubMed: 21878530]
41. Sorensen BS, Alsner J, Overgaard J, Horsman MR. Hypoxia induced expression of endogenous markers in vitro is highly influenced by pH. Radiother Oncol. 2007; 83(3):362–366. [PubMed: 17512623]
42. Vegran F, Boidot R, Michiels C, Sonveaux P, Feron O. Lactate Influx through the Endothelial Cell Monocarboxylate Transporter MCT1 Supports an NF-{kappa}B/IL-8 Pathway that Drives Tumor Angiogenesis. Cancer Res. 2011; 71(7):2550–2560. [PubMed: 21300765]
43. Brown JM, Giaccia AJ. The unique physiology of solid tumors: opportunities (and problems) for cancer therapy. Cancer Res. 1998; 58(7):1408–1416. [PubMed: 9537241]
44. Primeau AJ, Rendon A, Hedley D, Lilge L, Tannock IF. The distribution of the anticancer drug Doxorubicin in relation to blood vessels in solid tumors. Clin Cancer Res. 2005; 11(24 Pt 1):8782–8788. [PubMed: 16361566]
45. Seth P, Grant A, Tang J, Vinogradov E, Wang X, Lenkinski R, Sukhatme VP. On-target inhibition of tumor fermentative glycolysis as visualized by hyperpolarized pyruvate. Neoplasia. 2011; 13(1):60–71. [PubMed: 21245941]

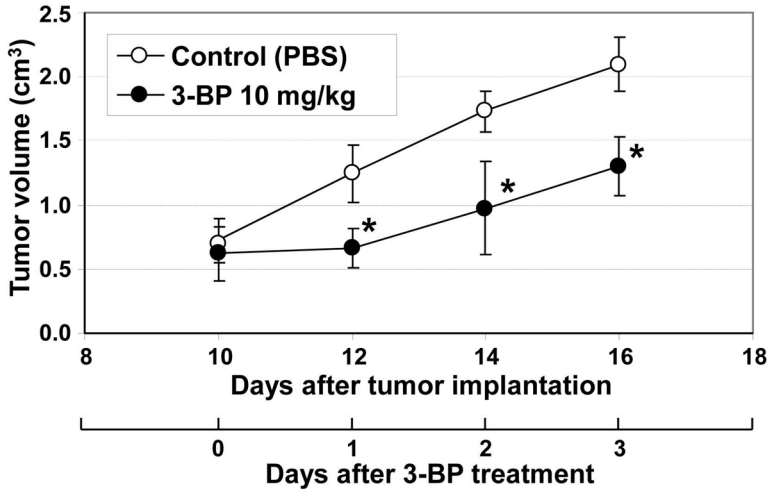

Figure 1.

Daily administration of 3-BP delayed SCC tumor growth. When tumor size became 1.0-1.2 cm (10 days after implantation), 10 mg/kg/day of glycolysis inhibitor 3-BP was intraperitoneally injected into mice bearing SCC tumor on their right leg. The 3-BP significantly suppressed the SCC tumor growth compared to control group of mice treated by PBS as vehicle.

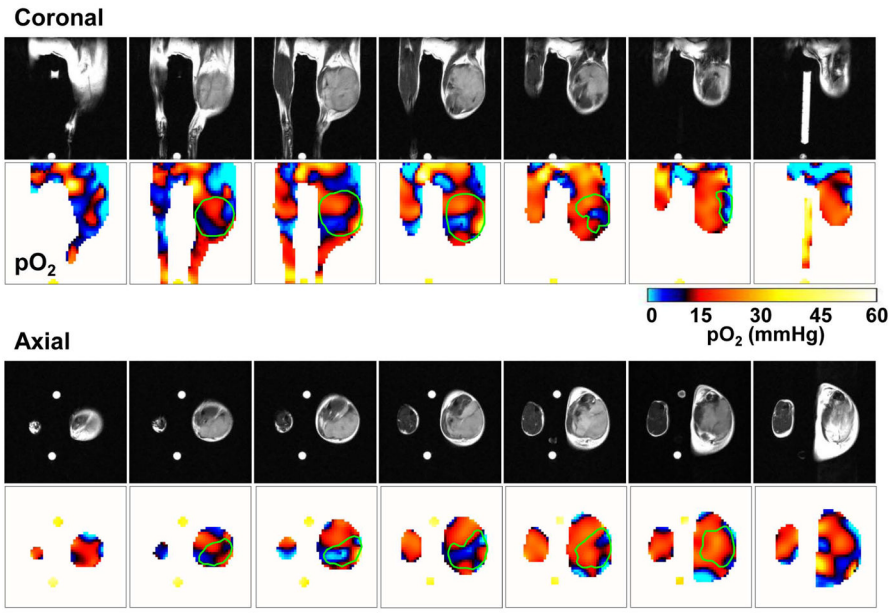

Figure 2.
Three-dimensional oxygen maps in a SCC tumor from EPRI. Oximetric images of a mouse bearing SCC tumor were acquired by EPRI at 10 mT. Sequentially, anatomic images were obtained by T_2-weighted 7T MRI. Both MRI and EPRI scans were performed using an identical coil operating at 300 MHz without removing the mouse from coil assembly. The coronal and axial sliced images were serially displayed at every 2 mm.

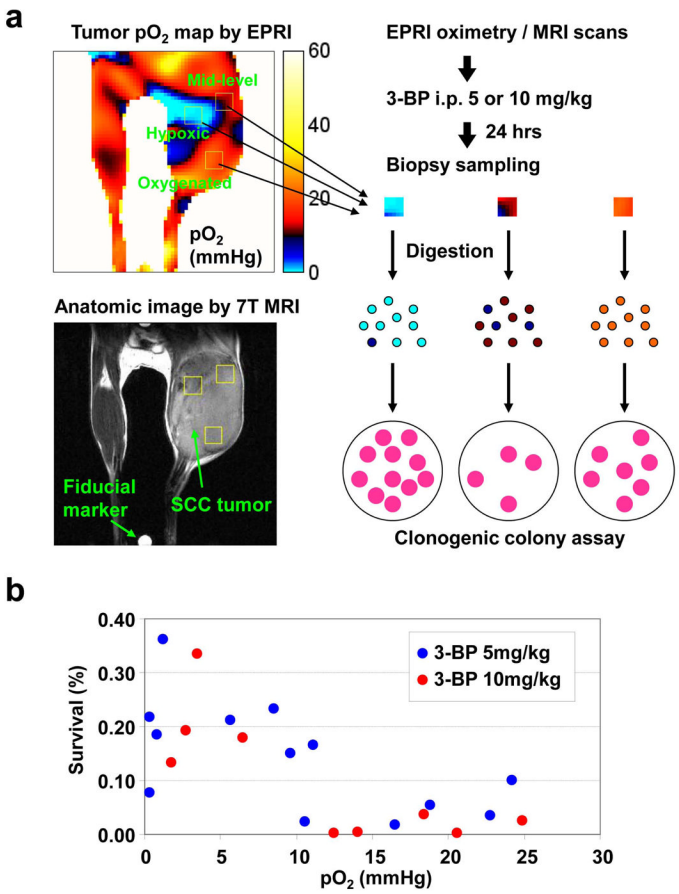

Figure 3.

Anti-tumor effect of 3-BP was attenuated in the hypoxic regions. (a) After EPR oxygen imaging and following anatomic imaging with MRI, tumor-bearing mice were intraperitoneally received 5 or 10 mg/kg of 3-BP. Biopsy samples were obtained from specific tumor regions to have different levels of oxygen concentration based on the anatomy-coregistered oxygen maps 24 hrs after 3-BP injection. The biopsy samples were digested by collagenase solution and applied to clonogenic colony assay for evaluating anti-tumor effect of 3-BP. (b) Scatter plots of local tumor pO_2 values and *in vivo* clonogenic cell survival of biopsy samples 24 hrs after 3-BP administration.

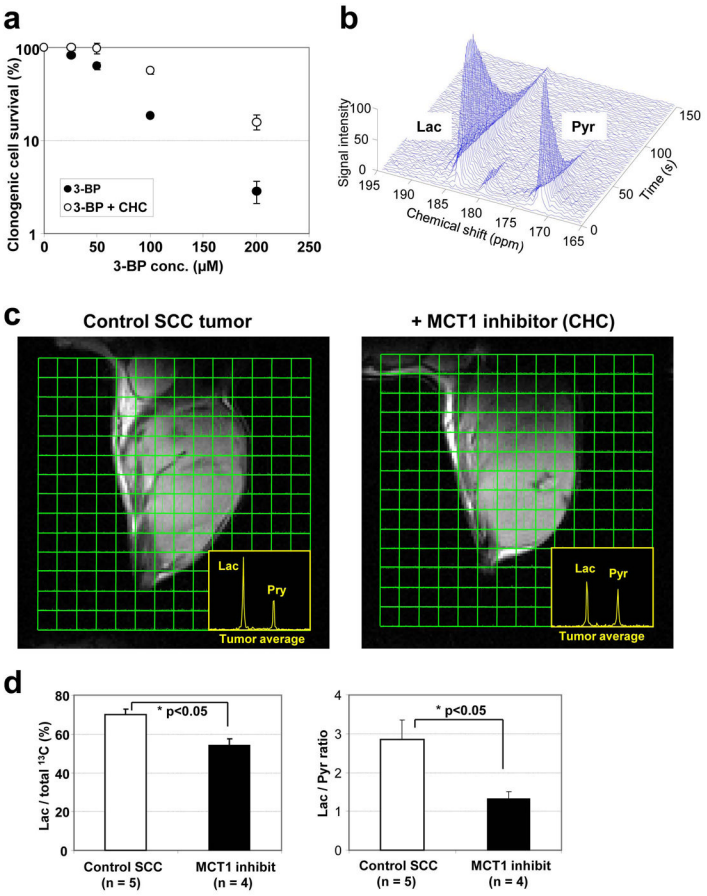

Figure 4.

3-BP enters cells via MCT1 in SCC tumor. (a) *In vitro* clonogenic cell survival assay in the presence of MCT1 inhibitor CHC. (b) ^{13}C MR spectroscopy of metabolites after intravenous injection of hyperpolarized ^{13}C-labeled pyruvate in a SCC tumor. (c) Metabolic ^{13}C MRI of hyperpolarized ^{13}C-labeled pyruvate in SCC tumors with or without pretreatment of CHC obtained 30 s after ^{13}C-pyruvate injection. (d) Pretreatment of MCT1 inhibitor CHC significantly suppressed lactate/total ^{13}C and lactate/pyruvate ratios calculated from whole tumor regions in ^{13}C MRI images.

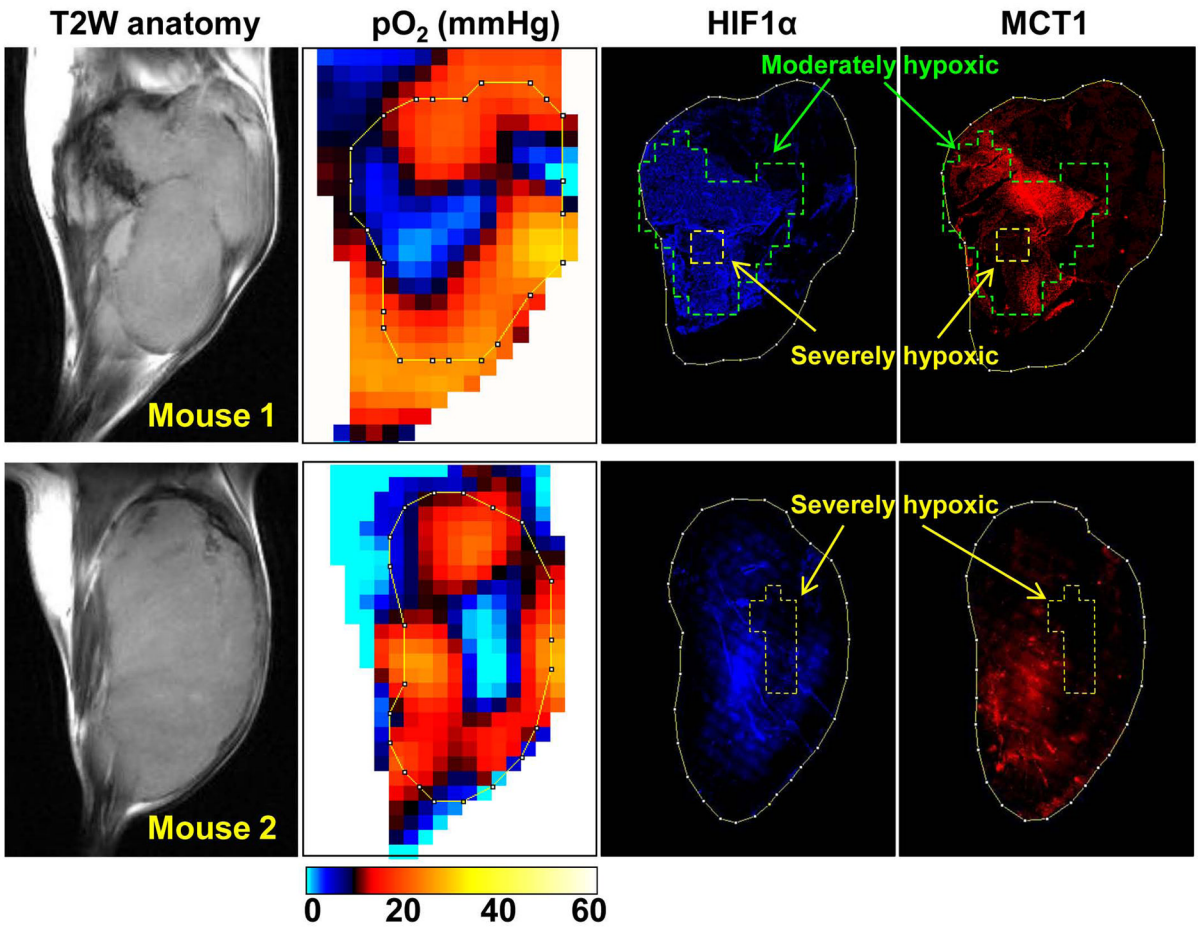

Figure 5.

Comparison of tumor pO_2 and MCT1 expression *in vivo*. After EPR oxygen imaging and following anatomic MRI scans, tumor tissue slice corresponding to the particular slice of pO_2 map was exsected, and immunestaining of HIF-1a (blue) and MCT1 (red) was conducted.